Molecular Crystals and Liquid Crystals
Publication details, including instructions for authors and subscription information:
http://www.tandfonline.com/loi/gmcl16

Overhauser Shift of the Conduction Electron Spin Resonance in $(FA)_2PF_6$ Single Crystals

W. Stöcklein [a] & G. Denninger [a]
[a] Physikalisches Institut and Bayreuther Institut für Makromolekülforschung (BIMF), Universität Bayreuth, POB 3008, D-8580, Bayreuth, West Germany
Version of record first published: 20 Apr 2011.

To cite this article: W. Stöcklein & G. Denninger (1986): Overhauser Shift of the Conduction Electron Spin Resonance in $(FA)_2PF_6$ Single Crystals, Molecular Crystals and Liquid Crystals, 136:2-4, 335-360

To link to this article: http://dx.doi.org/10.1080/00268948608074734

Mol. Cryst. Liq. Cryst., 1986, Vol. 136, pp. 335–360
0026-8941/86/1364–0335/$25.00/0

Printed in the United States of America

Overhauser Shift of the Conduction Electron Spin Resonance in $(FA)_2PF_6$ Single Crystals

W. STÖCKLEIN and G. DENNINGER

Physikalisches Institut and Bayreuther Institut für Makromolekülforschung (BIMF), Universität Bayreuth, POB 3008, D-8580 Bayreuth, West Germany

(*Received October 17, 1985*)

The shift ΔB_{ov} of the ESR line due to saturation of the NMR of the hyperfine coupled nuclei (Overhauser shift) was measured for single crystals of the organic conductor $(FA)_2PF_6$. ΔB_{ov} is proportional to $\overline{A}_{zz}$, being the average hyperfine interaction between the conduction electrons and the protons in resonance, and the dynamic nuclear spin polarization (DNP), respectively. The DNP enhancement factor V was determined for the two orientations of the static magnetic field B_o, perpendicular ($V_\perp = 525 \pm 40$) and parallel ($V_\parallel = 280 \pm 25$) to the needle axis a, respectively. The absolute value of the average hyperfine coupling is $\overline{A}_{zz} = -(1.16 \pm 0.05)$ Gauss $\cdot g_e\mu_B$. Both, the temperature dependence and the anisotropy of the proton spin relaxation times T_1^p and T_2^p were measured from the time dependence of the Overhauser shift, $\Delta B_{ov}(t)$ after *rf*-pulses or after switching "on" and "off" the ESR saturation. Within the metallic phase of the crystal the proton relaxation is governed by a Korringa law. The experiments definitely show, that the electron spins, showing up in the ESR are those of the conduction electrons.

I. INTRODUCTION

Single crystals of difluoranthenylphosphorhexafluoride, $(FA)_2^+PF_6^-$ (Figure 1), belong to the class of one-dimensional organic conductors, the organic part of which are pure aromatic hydrocarbons.[1–4] At room temperature they are highly conducting single crystals[5] showing a quasi metallic phase for $T > T_c = 190$ K, and a semiconducting phase below T_c.[6–8] Above T_c the conductivity is highly anisotropic ($\sigma_\parallel/\sigma_\perp \approx 100$); below T_c this anisotropy is reduced to a value less than 10. The crystal structure was investigated by Enkelmann:[9,10] the lattice is monoclinic ($a = 6.61$ Å, $b = 12.57$ Å, $c = 14.77$ Å, $\beta = 104°$);

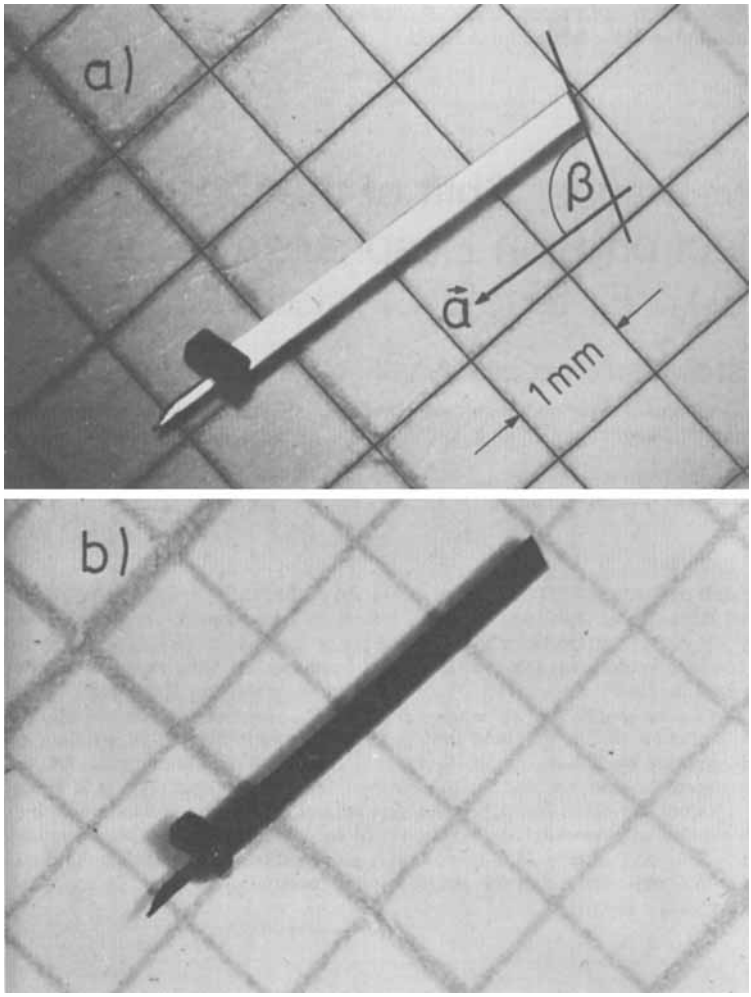

FIGURE 1 As grown $(FA)_2PF_6$ single crystal under two different illuminating directions:

a) specular reflection of the visible light
b) off the specular angle.

The crystal, as usual, was grown electrochemically; the position of the electrode was at its lower left sharp end.
See Color Plate V.

the fluoranthene molecules (FA = $C_{16}H_{10}$) are stacked along a, their molecular plane being oriented perpendicular to a. Their average distance along a is 3.3 Å, but they are slightly dimerized already for $T > T_c$. The counterions PF_6^-, being closed shell systems, are situated in segregated stacks between the FA stacks which carry the conduction electrons.

One of the most striking features of these crystals is their ESR spectrum,[6] which for $T > T_c$ is due to the conduction electrons: crystals of a mass of only about 100 μg show a very strong ESR signal, the width of which is only 10 mGauss or less.[5] This strong motional narrowing has initiated a series of interesting ESR experiments: electron spin relaxation and charge carrier diffusion have been investigated by both, cw- and time resolved ESR for electron Larmor frequencies ranging from 4.4 MHz to 9.5 GHz.[5,7,11,12] Even a few experiments for 90 GHz have been carried out.[23]

The charge carrier diffusion constants $D_\parallel$ and $D_\perp$ for diffusion parallel and perpendicular to a, respectively have been measured by the electron spin echo (ESE) technique by Maresch et al.[11,13] and, independently, by Stöcklein and Schiller:[14,15] $D_\parallel = 2\ \mathrm{cm^2\ s^{-1}}$, $D_\parallel/D_\perp \approx 1000$.[15]

The nuclear spin relaxation has been investigated by Höptner et al.[16,31] From both, the frequency dependence of the longitudinal proton spin relaxation time T_1^ρ and from the diffusion constants $D_\parallel$ and $D_\perp$ a time τ^* has been estimated, after which the charge carriers terminate their one dimensional motion: $2.2 \cdot 10^{-12}\ \mathrm{s} < \tau^* < 4.4 \cdot 10^{-12}$ s. This termination could be due either to an incoherent motion perpendicular to a or to a charge carrier trapping within the one-dimensional stack. The scattering time $\tau_\parallel$, characterizing the motion within the one-dimensional stack was determined to be ranged between $3 \cdot 10^{-15}$ s and $7 \cdot 10^{-14}$ s, the correct value being dependent on the model by which the motion is described.[13,14,17]

In order to be able to analyze further properties of the charge carriers in these organic conductors on the basis of experiments in single crystals we have developed the Overhauser shift method to be described below. This method investigates details of the hyperfine interaction between the charge carriers and magnetic nuclei in spite of the strong motional narrowing of the ESR. It is a complementary method to Knight shift experiments and has a very high sensitivity. So far the electron proton interaction has been investigated extensively.[14,18] But the Overhauser shift due to ^2H and ^{13}C also has been detected.[19]

It will be shown that the results not only have to be taken into

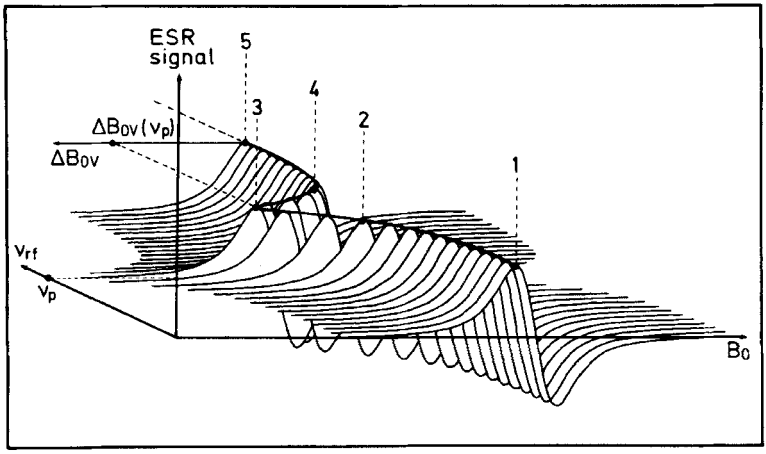

FIGURE 2 The principle of the Overhauser shift experiment. In addition to the microwave field with frequency $\nu_{\mu w}$ = const. (e.g. 9.6 GHz) the sample is irradiated with a radio frequency field with frequency ν_{rf}. The external magnetic field B_o is varied as in a conventional ESR experiment. In the Figure ν_{rf} is a parameter. If $\nu_{rf} \ll \nu_p$ the ordinary *cw*-ESR line is detected (1). ν_p is the proton Larmor frequency. For $\nu_{rf} \rightarrow \nu_p$ the ESR line is shifted (2). This shift is called Overhauser shift ΔB_{ov}. If $\nu_{rf} = \nu_p$ ΔB_{ov} shows its maximum value $\Delta B_{ov}(\nu_p)$ (3). For $\nu_{rf} > \nu_p$ the shift vanishes, i.e. the ESR line shows its original position (5).

After switching off the radio frequency field with $\nu_{rf} = \nu_p$ (3) the relaxation of the Overhausershift, $\Delta B_{ov}(t)$ can be observed directly (see Chap. IV).

account for the determination of the electronic structure of the organic conductors but also for their application as Gaussmeters.[20] Finally the experiments will show that extreme care has to be taken in analyzing the shape of the wings of narrow ESR lines, because these ESR lines can become considerably asymetric due to the Overhauser shift.

II. OVERHAUSER SHIFT ΔB_{ov}

Line 1 in Figure 2 shows a conventional *cw*-ESR signal of an $(FA)_2^+PF_6^-$ single crystal. The line width at room temperature is $\Delta B_{pp} \approx 10$ mG; the averaged *g*-value is $\bar{g}_e \approx 2.00236$ (see below). The microwave frequency for our experiments was $\nu_{\mu w} \approx 9.6$ GHz. For the additional lines in Figure 2 (. . . 2 . . . 3 . . . 4 . . . 5) the sample was irradiated in addition to the microwave field with a radio frequency field, the frequency of which was ν_{rf}. If ν_{rf} approaches the proton Larmor frequency ν_p a shift of the *cw*-ESR line is observed (2). We call this shift Overhauser shift $\Delta B_{ov}(\nu_{rf})$. It reaches its max-

imum value $\Delta B_{ov}(\nu_p)$ if $\nu_{rf} = \nu_p(3)$. $\Delta B_{ov}(\nu_p)$ is of the order of several milligauss (see below). For ν_{rf} sufficiently above ν_p the cw-ESR position again reaches its original value, i.e. $\Delta B_{ov} = 0$ (5).

In 1953 Overhauser has predicted this shift for metals at low temperatures.[24] For lithium it was observed at very low temperatures by Ryter.[25,26] For organic conductors it was mentioned by Sanny and Clark.[27] Detailed investigations of the effect as well as its application to the best knowledge of the authors are not known but will be given in the present paper. First results have been published earlier.[18]

The Overhauser shift $\Delta B_{ov}(\nu_{rf})$ of the conduction electron spin resonance line is due to switching off the nuclear field by saturating the NMR. The nuclear field is the sum of the nuclear fields of all nuclei of the crystal. For a first order approximation let us regard the N protons per conduction electron within the $(FA)_2PF_6$ crystal as being equivalent: $N = 20$. They produce a longitudinal nuclear field

$$\Delta B_p = 1/2\, \overline{A}_{zz} \cdot N \cdot \mathcal{P} \cdot 1/g_e\mu_B \tag{1}$$

$\overline{A}_{zz}$ is the averaged z-component of the hyperfine tensor of the protons, z the direction of the external field B_o and $\mathcal{P} = (n_+ - n_-)/(n_+ + n_-)$ is the average proton nuclear spin polarization, n_+ and n_- being the total numbers of proton spins up and down, respectively. If the proton spins are in thermal equilibrium at $T = 300$ K and in an external field of $B_o = 3300$ G the proton spin polarization becomes $\mathcal{P} = \mathcal{P}_o$:

$$\mathcal{P}_o = \tanh(g_e \cdot \mu_B B_o/2kT) = 1.1 \cdot 10^{-6} \tag{2}$$

This small nuclear spin polarization will shift the center of the motionally narrowed *cw*-ESR line with respect to the "pure g_e position". The size of the shift according to (1) and (2) is of the order of 10^{-5} of the average hyperfine splitting which would be observed in absence of motion, i.e. for resolved hyperfine splitting in the isolated radical. Thus, the Overhauser shift to be expected for proton spins in thermal equilibrium is of the order of 10 μG.

However, if $\mathcal{P}_o$ is amplified by dynamic nuclear spin polarization (DNP) via ESR saturation (Overhauser effect), ΔB_p can reach values comparable to the ESR line width in $(FA)_2PF_6$. For pure isotropic hyperfine coupling the maximum value of $\mathcal{P}$ is

$$\mathcal{P}_{max} = \mathcal{P}_o(1 + \gamma_e/\gamma_p) \approx \mathcal{P}_o \cdot 658 \tag{3}$$

(γ_e and γ_p = gyromagnetic ratios of electron and proton respectively).

The amplification of $\mathcal{P}_o$ via DNP now will be treated in the frame of a two spin model. The four levels as usual are indicated by $|m_I, m_s>$ (e.g. $|-,+>$ indicates $m_I = -1/2$ and $m_s = +1/2$). The rate constants w characterize the different transitions as follows:

w_1 for $\Delta m_I = \pm 1, \Delta m_s = 0$ transitions $(|-, m_s> \leftrightarrow |+, m_s>)$

w_0 for $\Delta m_I = \pm 1, \Delta m_s = \mp 1$ flip-flop processes

$$(|+,-> \leftrightarrow |-,+>)$$

w_2 for $\Delta m_I = \pm 1$ and $\Delta m_s = \pm 1$ flip-flip processes

$$(|+,+> \leftrightarrow |-,->).$$

The z-component of I in this approximation is described by the following rate equation.[28]

$$\frac{dI_z}{dt} = -(w_0 + 2w_1 + w_2 + w^\circ)(I_z - I_0) - (w_2 - w_0)(S_z - S_o) \quad (4)$$

w° subsummerizes all relaxation processes, which are not due to hyperfine interaction with the conduction electron system. A steady state solution ($dI_z/dt = 0$) of (4) is

$$I_z = I_0 + \frac{w_2 - w_0}{w^t}(S_o - S_z) \quad (5)$$

with $w^t = w_0 + 2w_1 + w_2 + w^\circ = 1/T_1^p$.

(5) can be written in the following form:

$$I_z = I_o\left\{1 + \frac{w_2 - w_0}{w_0 + 2w_1 + w_2} \cdot \frac{w_0 + 2w_1 + w_2}{w^t} \cdot \frac{S_o - S_z}{S_o} \cdot \frac{S_o}{I_o}\right\} \quad (6)$$

or

$$I_z = I_o\{1 + \xi \cdot f \cdot S \cdot \gamma_e/\gamma_p\} \quad (7)$$

(ξ = coupling parameter, f = leakage factor, S = saturation parameter). With (7) the nuclear spin polarization becomes

$$\mathcal{P} = \mathcal{P}_o \cdot (1 + \xi \cdot f \cdot S \cdot \gamma_e/\gamma_p) = \mathcal{P}_o \cdot (1 + VS) \tag{8}$$

In the following we call $V = \xi \cdot f \cdot \gamma_e/\gamma_p$ the enhancement factor.

In the experiment, described above, we observe the nuclear field with inversed sign as the Overhauser shift, because the NMR saturation switches off the nuclear field:

$$\Delta B_{ov} = -\Delta B_p \tag{9}$$

Equation (1) shows that the experiment yields the product $\overline{A}_{zz} \cdot \mathcal{P}$. We will show below that V and S can be determined experimentally. Thus, $\overline{A}_{zz}$ can be determined. This quantity directly yields the density of the charge carriers within the carbon framework.[29]

But also $\mathcal{P}(t)$ can be determined if the Overhauser shift experiment is made time dependent. This time dependence of $\mathcal{P}$ is described by (4). We have to distinguish two limiting cases which can be realized experimentally:

1. The electron spin system is in thermal equilibrium ($S = 0$)
2. The electron spin system is saturated ($S = 1$).

For the first case ($S_z = S_o$) we find from (4) for $I_z(0) \neq I_o$:

$$I_z - I_o = I_z(0) \cdot \exp(-(w_0 + 2w_1 + w_2 + w^\circ)t) \tag{10}$$

and thus the longitudinal relaxation rate for the protons:

$$1/T_1^p = w_0 + 2w_1 + w_2 + w^\circ \tag{11}$$

For the second case ($S_z = 0$) we find from (5) the steady state nuclear spin polarization I_z^{DNP}

$$I_z^{\mathrm{DNP}} = I_o + S_o(w_2 - w_0)/(w_0 + 2w_1 + w_2 + w^\circ) \tag{12}$$

and the time dependence of the DNP

$$I_z(t) = I_z^{\mathrm{DNP}} \cdot (1 - \exp(-(w_0 + 2w_1 + w_2 + w^\circ)t)) \tag{13}$$

This time dependence can be observed directly in the Overhauser shift experiment after switching off the *rf* field. The relevant rate constant is the longitudinal proton spin relaxation rate $1/T_1^p$.[11]

III. EXPERIMENTAL

All the experiments have been performed with a commercial ESR spectrometer (Bruker ER 200D-SRC) equipped with an ENDOR cavity ($\nu_{\mu w}$ = 9.6 GHz); the maximum microwave power was P_0 = 300 mW. Owing to the extremely narrow ESR line ($\Delta\nu_{pp}$ = 21.4 kHz), no AFC lock was used. Instead, the B_o field was locked to the frequency using a commercial field-frequency lock employing DPPH as a reference. Field modulation at a frequency of 6 kHz was employed with typical amplitudes of 2 mG. For the radio frequency generation, two arrangements were used alternatively: the *cw* mode used a Wavetek model 300 signal generator (1 – 250 MHz, resolution 1 kHz) amplified by an *rf* power amplifier (ENI 3100 L) delivering up to 100 W into 50 Ω. Standard AM modulation yields *rf* pulses as short as 10 μs. Shorter *rf* pulses were taken from a Bruker CXP-NMR spectrometer with power up to 1 kW into 50 Ω and pulse durations as short as 0.5 μs, yielding an effective B_2 of 0.48 G/W$^{1/2}$ for the ENDOR coil.

For reasons of sensitivity the following procedure for detecting $\Delta B_{ov}(\nu_{rf})$ was used. It is slightly different from the method described above and utilizes the strong slope in the center of the ESR signal, which as usual is the derivative of the ESR line. At first for $\nu_{rf} = 0$ the external field B_o is locked to the center of the ESR line: $B_o = B_{res}$. For this field the ESR signal is zero. Then the strong *rf* field is switched on and ν_{rf} is swept across the proton Larmor frequency range. The Overhauser shift ΔB_{ov}, which occurs during the saturation of the proton NMR is compensated by two extra coils attached to the cavity, the current in which is regulated such, that the ESR line remains locked to its center. Thus the current in these extra coils is directly proportional to ΔB_{ov} (ν_{rf}). Figure 3 shows as an example the Overhauser shift spectrum ΔB_{ov} (ν_{rf}) in the vicinity of the proton Larmor frequency ν_p. This mode of operation virtually eliminates problems of long-term stability of the spectrometer. All the experiments reported in the present paper employed this mode. Especially this is valid also for the time dependent experiments, detecting ΔB_{ov} (ν_p, t).

The $(FA)_2PF_6$ samples used in the investigations were tiny (~100 μg) single crystals. Temperature was controlled by means of the regulated flow of N_2 gas through the Dewar inside the cavity. The temperature regime covers the range from 100 K up to room temperature.

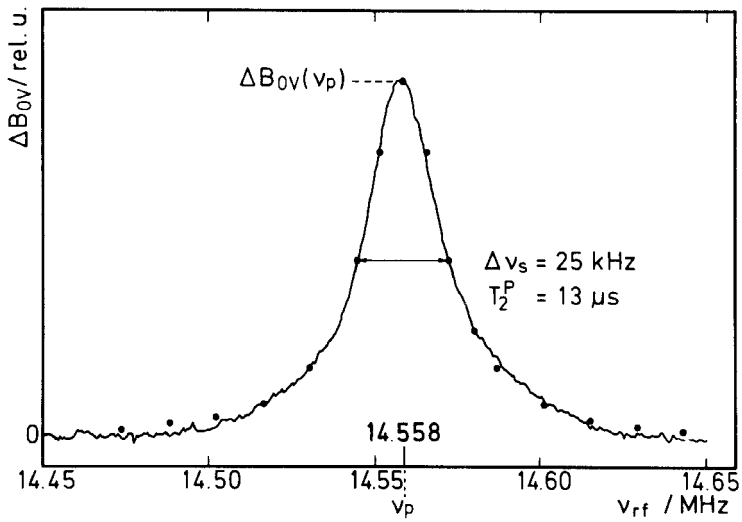

FIGURE 3 Overhauser shift ΔB_{ov} versus frequency ν_{rf} of the radio frequency field. ν_p = proton Larmor frequency. The drawn out line is the experimentally detected spectrum. $\Delta B_{ov}(\nu_p)$ for this experiment was about 3 mG. The dots represent a Lorentzian shaped NMR line corresponding to a width of $\Delta\nu_s$ = 25 kHz or a transversal proton spin relaxation time T_2^p = 13 μs, respectively.

IV. EXPERIMENTAL RESULTS

Determination of the enhancement factor *V*

Figure 3 shows the dependence of the Overhauser shift ΔB_{ov} on the radio frequency ν_{rf}, i.e. the NMR-spectrum as detected by the Overhauser shift. During this experiment both, the microwave power P and radio frequency power were kept constant. The radio frequency power was strong enough to saturate the NMR. The spectrum (Figure 3) shows a quasi Lorentzian line-shape (dots in Figure 3). The peak of this curve $\Delta B_{ov}(\nu_p)$ is proportional to the product $\overline{A}_{zz} \cdot \mathcal{P} = \overline{A}_{zz} \cdot \mathcal{P}_o \cdot (1 + V \cdot S) \approx \overline{A}_{zz} \cdot \mathcal{P}_o \cdot V \cdot S$ (if $V \cdot S \gg 1$ see (1) and (8)). We conclude from (1), (8) and (9):

$$V = \Delta B_{ov}(S = 1)/\Delta B_{ov}(S = 0) - 1 \qquad (14)$$

In our experiment both $S = 1$ and $S = 0$ are not completely accessible. But the measured dependence of ΔB_{ov} on microwave power P allows

a straightforward extrapolation to $S = 1$ and $S = 0$. In Figure 4a the experimental points follow very neatly the expected relation:

$$\Delta B_{ov} = (\Delta B_{ov})_{\max} \cdot \alpha P/(1 + \alpha P) = (\Delta B_{ov})_{\max} \cdot S \qquad (15)$$

where α is determined by the product $T_1^e \cdot T_2^e$ of the electron spin relaxation times and the factor relating B_1 with P. From (1), (8) and (9) and with the approximation $1 + V \cdot S \approx V \cdot S$ the ΔB_{ov} is found to be proportional to S:

$$\Delta B_{ov} = \Delta B_{ov}(S = 0) \cdot V \cdot S \qquad (16)$$

This dependence is shown in Figure 4b. The slope of the straight line

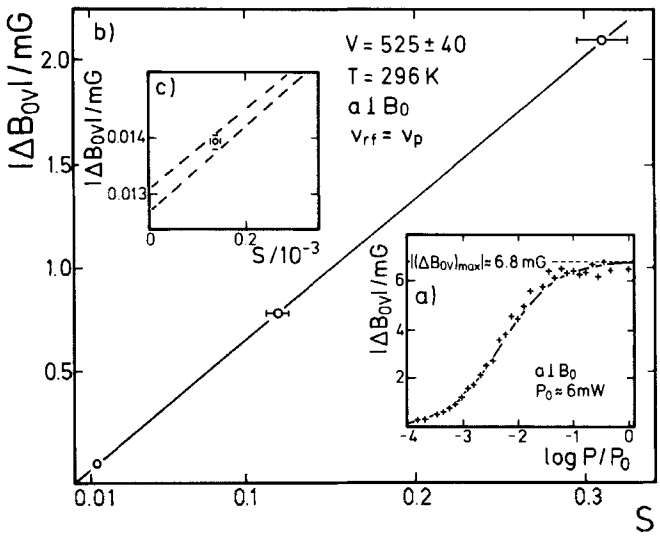

FIGURE 4 Determination of the enhancement factor V.

a) Overhauser shift $\Delta B_{ov}(\nu_p)$ versus power P of the microwave field. The power of the radio frequency field was strong enough to saturate the proton spin resonance completely. X: experimental values. Drawn out line: $\Delta B_{ov}(\nu_p) = (\Delta B_{ov})_{\max} \cdot S$.
b) $\Delta B_{ov}(\nu_p)$ versus (electron spin) saturation factor S. $S = \alpha P/(1 + \alpha P)$, α = const.$\cdot T_1^e \cdot T_2^e$. Dots: three experimental values which have been detected with highest achievable accuracy. Drawn out line: $B_{ov}(\nu_p) \propto S$.
c) $\Delta B_{ov}(\nu_p)$ versus S. Dot: experimental value for $S = 0.00014$, yielding $\Delta B_{ov}(\nu_p) = 0.0139$ mG. (Error bars: see figure). Dotted line: straight line with slope of b) (maximum and minimum value, respectively). From the ratio $\Delta B_{ov}(S = 1)/\Delta B_{ov}(S = 0)$ the enhancement factor V is calculated according to Eq. (14).

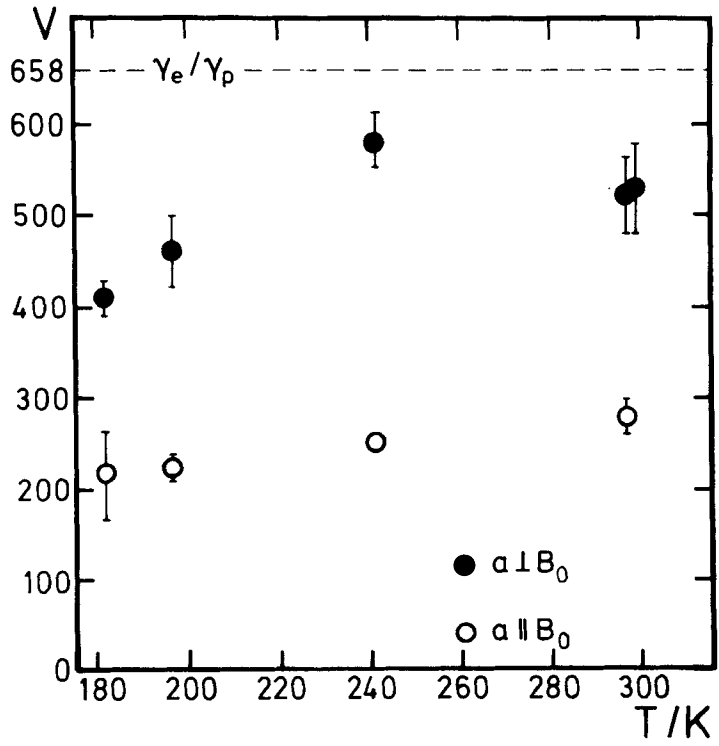

FIGURE 5 Temperature dependence of the enhancement factor V for two different orientations of the $(FA)_2PF_6$ crystal stack axis a with respect to the external field B_o.

is determined by two measurements at different microwave powers P_1 and P_2. Only the ratio P_1/P_2 had to be detected with high accuracy. Extrapolation of this line to $S = 1$ is straightforward.

A shift value ΔB_{ov} near $S = 0$ was determined by using extremely low microwave power. The extrapolation $S \rightarrow 0$ from this point with the slope of the straight line in Figure 4b yields the value ΔB_{ov} ($S = 0$) (see Figure 4c). For this experiment typical parameters have been: $P = 10^{-7}$ W, 10000 Scans, $S/N \approx 8$.

At $T = 296$ K, the enhancement factors $V_\perp$ and $V_\parallel$ were determined for the orientations a perpendicular and parallel to the static magnetic field: $V_\perp = 525 \pm 40$ and $V_\parallel = 280 \pm 20$. Figure 5 shows the temperature dependence of $V_\perp$ and $V_\parallel$ in the temperature region $180 < T < 300$ K.

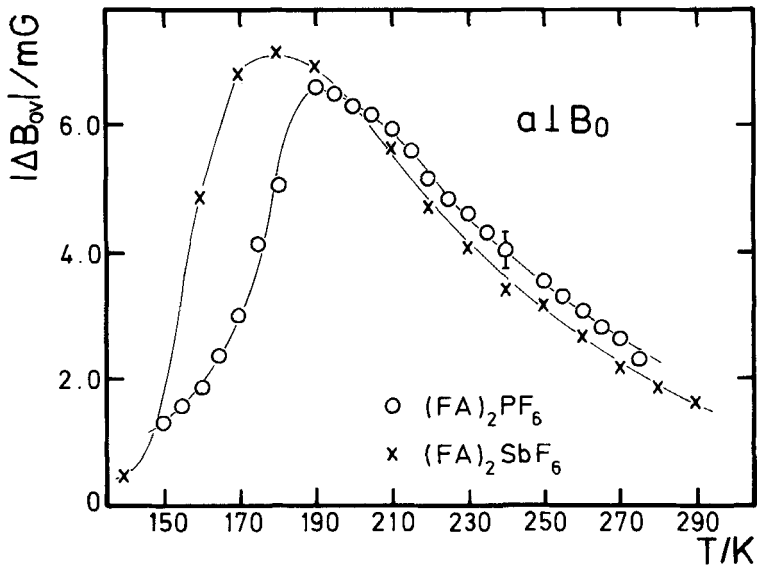

FIGURE 6 Temperature dependence of the Overhauser shift $\Delta B_{ov}(\nu_p)$ for $(FA)_2PF_6$ and for $(FA)_2SbF_6$, respectively. For this experiment the microwave power P was kept constant. For $T \sim 190$ K the $(FA)_2PF_6$ crystal shows a structural phase transition. For $T < 190$ K it behaves like a semiconductor.

Temperature dependence of ΔB_{ov}

The temperature dependence of the Overhauser shift ΔB_{ov} is shown in Figure 6 for different samples $(FA)_2PF_6$ and $(FA)_2SbF_6$. Just as the temperature dependence of the dc-conductivity[5] and of the magnetic susceptibility[5,22] the temperature dependence of the Overhauser shift is reflecting the phase transition at $T \approx 190$ K. Below room temperature ΔB_{ov} increases with decreasing temperature to its maximum value near $T \approx 190$ K. For $T < 190$ K ΔB_{ov} decreases steeply. For the interpretation of these data, which will be given later, it is necessary to know the values for $\mathcal{P}_0$, V and S.

Rotating the crystal around an axis which is perpendicular to both, the needle axis a and the static magnetic field B_o, the anisotropy of the Overhauser shift has been measured. For a $\perp B_o$ the Overhauser shift shows its maximum and for $a \| B_o$ its minimum value, respectively.

Longitudinal proton spin relaxation: T_1^p

The time dependence of the Overhauser shift $\Delta B_{ov}(t)$ has been detected after switching off the radio frequency power or after switching

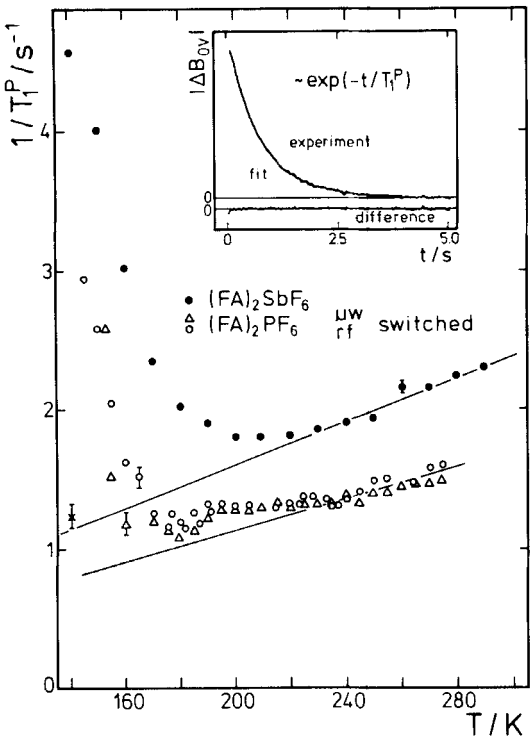

FIGURE 7 Temperature dependence of the relaxation of the Overhauser shift. Insert: Time dependence of the Overhauser shift: $\Delta B_{ov}(t)$ after switching off the ESR saturation at $t = 0$. The fit to $\Delta B_{ov} \propto \exp(-t/T_1^p)$ yields the longitudinal proton spin relaxation rates $1/T_1^p$. Drawn out straight lines: $T_1^p \cdot T = \text{const.}$ (Korringa law).

Switching off the *rf* power (open circles ○) yields the same values as switching off the microwave power (triangles △).

"on" and "off" the microwave power, respectively. The characteristic time constant deduced from this experiment is the longitudinal spin relaxation time of the protons (see Eq. (11) and Eq. (13) and chapter V). As shown in Figure 8 we observe within two decades a purely monoexponential decrease of the Overhauser shift after the *rf* is switched off. This is equivalent to a purely monoexponential increase of the DNP.

Figure 7 shows the temperature dependence of the longitudinal proton spin relaxation rate $1/T_1^p$ for two different crystals of $(FA)_2PF_6$ and for one $(FA)_2SbF_6$ crystal. For one of the $(FA)_2PF_6$-crystals $1/T_1^p$ has been determined by two different methods: either by switch-

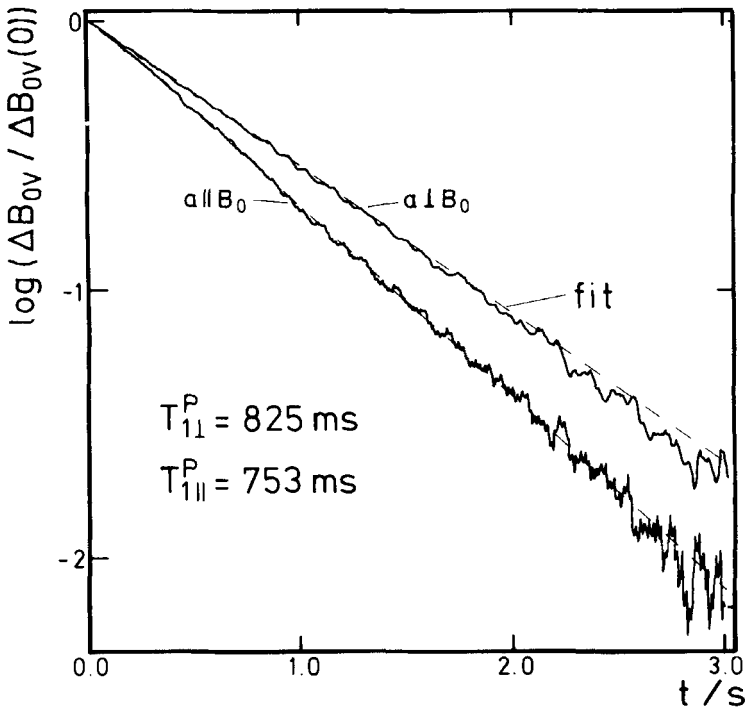

FIGURE 8 Anisotropy of the longitudinal proton spin relaxation for $(FA)_2PF_6$ ($T \approx 200$ K).

ing the *rf*-power (open circles ○) or by switching the microwave power. As shown in Figure 7 the results are identical.

In the temperature range between room temperature and 200 K, the data were fit with straight lines which cross the origin ($T = 0$, $1/T_1^p = 0$).

Because of the high accuracy of the measurement of $\Delta B_{ov}(t)$ it was possible to determine the anisotropy of the proton spin relaxation rate constant $1/T_1^p$. Figure 8 shows $\Delta B_{ov}(t)$ on a logarithmic scale for the orientations a $\perp B_o$ and a $\parallel B_o$. For $T > 190$ K the ratio $(T_1^p)_\perp / (T_1^p)_\parallel$ is constant: $(T_1^p)_\perp / (T_1^p)_\parallel = 1.15 \pm 0.025$.

Transverse proton spin relaxation

In addition to T_1^p the transverse proton spin relaxation has been determined with three different methods.

Figure 3 shows a proton NMR spectrum as detected by the Overhauser shift method. The linewidth of the quasi Lorentzian line

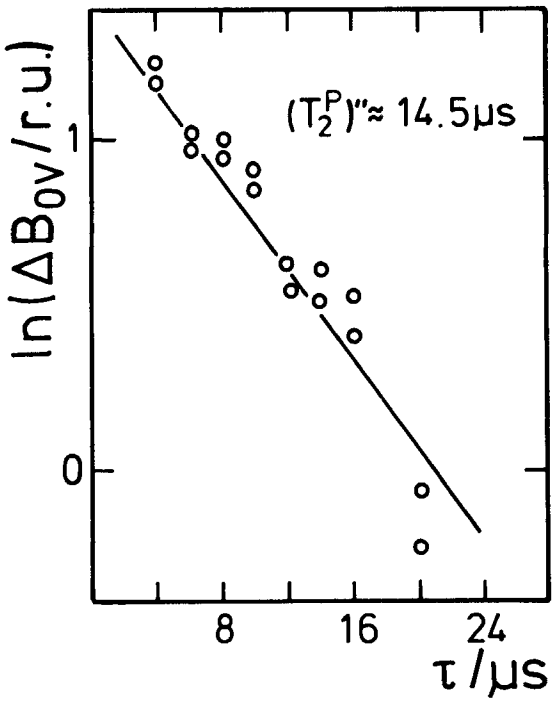

FIGURE 9 Determination of the transversal proton spin relaxation time $(T_2^p)^{\parallel}$. ΔB_{ov} was detected immediately after a 90°–τ–90° proton spin pulse sequence.

is $\Delta\nu_s$ = 25 kHz. This would correspond to a transverse proton spin relaxation time T_2^p = (13 ± 1) μs.

By irradiation of *rf* pulses the magnetization vector of the nuclei can be rotated in the rotating frame of the nuclei as usual in pulsed NMR spectroscopy. For example, by applying a 180° pulse the magnetization vector and consequently the DNP can be inverted, followed by an exponential return to the steady-state value. By application of an *rf* pulse (1 kW, duration τ = 1 − 50 μs), transient nutation of the DNP is observed. From this experiment we deduced the decay time of the transverse proton magnetization as $(T_2^p)'$ = (16 ± 3) μs.[18]

The pointwise detection of the proton FID via the Overhauser shift yields a third method to determine T_2^p. A 90° pulse rotates the magnetization vector of the proton spin system to the x'-y'-plane. For classical NMR we now would detect the signal (FID) which would be induced in a detector coil. But the Overhauser shift is only detectable if one component of the magnetization is parallel to the z-axis. Therefore, after the time interval τ for which the magnetization

has to be detected it has to be turned back to the z-direction by a further 90° pulse. During the time interval τ between the two *rf* pulses transverse proton spin relaxation occurs, which causes a reduced value of the shift $\Delta B_{ov}(\tau)$ at the time τ.

Subsequent variation of the time interval τ and detection of the Overhauser shift $\Delta B_{ov}(\tau)$ yields the pointwise scanned FID (Figure 8). Evaluation of the decaytime yields: $(T_2^p)^{\parallel} = (14.5 \pm 1)$ μs.

V. DISCUSSION

Hyperfine interaction

The proton Overhauser shift is negative: $B_{res}(\nu_p) - B_{res}(o) = \Delta B_{ov}(\nu_p) < 0$. Therefore the average hyperfine coupling constant also is negative: $\overline{A}_{zz} < 0$. Taking into account the experimental values $V = +525$, $S = 1$ and $\Delta B_{ov} = -6.8$ mG, respectively, we calculate by (1) and (8): $\overline{A}_{zz}/g_e\mu_B = -(1.16 \pm 0.05)$ G. Both, the sign and the absolute value of $\overline{A}_{zz}$ are characteristic for π-electrons in aromatic hydrocarbons.[29] With an averaged spin density $1/N$ ($N = 20$) and the experimental value of $\overline{A}_{zz}$ the McConnell relation[29] yields: $Q = -22$ Gauss which is a typical value for aromatic hydrocarbons.

Anisotropy of the Overhauser shift

For the following discussion we assume that the hyperfine coupling to a first order is isotropic. For this approximation the anisotropy of ΔB_{ov} is determined by $V = \xi \cdot f \cdot \gamma_e/\gamma_p$ and S, respectively. The experimental result was $(\Delta B_{ov})_{\perp}/(\Delta B_{ov})_{\parallel} \approx 2$, $\perp$ and $\parallel$ indicating the orientation of B_o with respect to a. Thus, for $S = 1$

$$V_{\perp}/V_{\parallel} \approx 2 \tag{17}$$

The leakage factor f is only slightly different from unity. We therefore assume $f = 1$, which means that $\xi = (w_2 - w_0)/(w_0 + 2w_1 + w_2)$ must be strongly anisotropic. I.e. the values of w_i are dependent on the orientation of B_o. For both orientations, $\perp$ and $\parallel$, and for the entire temperature range 145 K $< T <$ 300 K, respectively the enhancement factor is positive: $V > 0$. As $\gamma_e/\gamma_p < 0$, ξ also must be negative, i.e. $w_2 < w_0$! As the values of w_i are anisotropic, the values of $1/T_1^p = w_0 + 2w_1 + w_2$ also must be anisotropic. This indeed has been observed (Figure 8). Having in mind the four experimental

values $V_\parallel$, $V_\perp$, $(1/T_1^p)_\parallel$ and $(1/T_1^p)_\perp$, respectively we find from (5, 6) the following relations:

$$\xi_\perp = \frac{(\tilde{w}_2)_\perp - 1}{1 + (\tilde{w}_1)_\perp + (\tilde{w}_2)_\perp} \tag{18a}$$

$$\xi_\parallel = \frac{(\tilde{w}_2)_\parallel - 1}{1 + (\tilde{w}_1)_\parallel + (\tilde{w}_2)_\parallel} \tag{18b}$$

$$\frac{(T_1^p)_\perp}{(T_2^p)_\parallel} = \frac{1 + (\tilde{w}_1)_\parallel + (\tilde{w}_2)_\parallel}{1 + (\tilde{w}_1)_\perp + (\tilde{w}_2)_\perp} \tag{18c}$$

where $\tilde{w}_1 = 2w_1/w_0$ and $\tilde{w}_2 = w_2/w_0$ are relative rate constants for the orientations indicated in (18a–18c). With the experimental values of V and T_1^p (see above) we find $(\tilde{w}_1)_\perp = 0.32$, $(\tilde{w}_2)_\parallel = 0.46$, $(\tilde{w}_1)_\parallel \approx (\tilde{w}_2)_\perp = 0$. It should be mentioned here once more that these values represent a rough estimation; but they seem to be reasonable as will be shown in the following discussion.

Let us regard the Hamiltonian for magnetic dipolar coupling in its commonly used form as a sum of six components A, B, C, D, E and F respectively.[30] These components show a different anisotropy. w_2 and w_1 belong to those components, which are proportional to $\sin^2 \theta_i$ and $\sin \theta_i \cos \theta_i$, respectively. θ_i is the angle between the electron proton distance and the magnetic field B_o, respectively. For $a \parallel B_o$ all $\theta_i = 90°$. I.e. the components E and F, both containing $\sin^2 \theta_i$ reach their maximum values. The terms C and D vanish ($\cos \theta_i = 0$). Therefore $(w_2)_\parallel$ is "large" and $(w_1)_\parallel = 0$, as observed experimentally! For $a \perp B_o$ all θ_i are different. The sum over all components containing $\sin^2 \theta_i$ is therefore smaller than the corresponding sum for $a \parallel B_o$. On the other hand the components C and D now become unequal zero. Thus for $a \perp B_o$ we expect $(w_2)_\perp \ll (w_2)_\parallel$ and $(w_1)_\perp \neq 0$, as observed experimentally!

This discussion has shown, that both, the large anisotropy of the Overhauser shift and the small anisotropy of T_1^p qualitatively are described correctly by the dipolar hyperfine interaction. It also shows that the isotropic part of the proton spin relaxation exceeds the anisotropic part considerably.

Proton spin relaxation

The rate constants for both, the increase and the decrease of the DNP according to (11 and 13) are expected to be identical and equal

to the longitudinal proton spin relaxation rate $1/T_1^p$. This also has been shown experimentally (Figure 6). The advantage using $\Delta B_{ov}(t)$ instead of conventional NMR for the detection of T_1^p is due to the large enhancement factor V and probably also due to the higher quantum energy of the microwaves as compared to the *rf*-radiation.

The temperature dependence of T_1^p as detected via $\Delta B_{ov}(t)$ for a small single crystal (Figure 7) is in agreement with the temperature dependence which has been published by Höptner et al.[16,31] for a large powder sample. The analysis in Figure 10 shows that $1/T_1^p$ can be regarded as a sum of three terms:

1. the relaxation rate due to the proton-electron interaction,
2. the relaxation rate due to the proton-fluor interaction and
3. the relaxation rate due to paramagnetic imperfections.

For the quasi metallic temperature region, i.e. for $T > 190$ K the relaxation due to conduction electrons dominates: it is described by a Korringa law. The validity of a Korringa law is the strongest proof that the observed ESR line is due to the spins of the charge carriers. But it should be noted, that compared to the classical metals the ESR susceptibility of $(FA)_2PF_6$ is not really constant in this temperature region; its variation is only about 20%.[22] Therefore $T_1^{PE} \cdot T = \text{const.}$ is not fullfilled exactly (Figure 10).

Decay constants between 13–16 μs as detected by the Overhauser shift for the transversal magnetization are comparable to the value $T_2 \approx 10$ μs (Höptner et al.)[16] and 12–15 μs (Sachs et al.)[17] determined by conventional NMR for powder samples. The Overhauser shift spectrum $\Delta B_{ov}(\nu_{rf})$ seems to consist of a homogeneous line (Figure 3). The corresponding proton resonance linewidth of 25 kHz (~6 G) is typical for solids where dipolar interaction between the nuclei is dominant.

A broadening of the NMR line due to inhomogeneities in the B_o field can be ruled out for our small sample volume, since the relative width of the ESR signal is $3 \cdot 10^{-6}$. Inhomogeneities in the magnetic field of the *rf* field have not been observed.

In partially deuterated crystals (contents of protons $\approx 10\%$) the proton resonance line width is reduced by more than a factor of two as compared to its linewidth in pure protonated crystals. This fact shows the essential contribution of the dipolar interaction to the linewidth of the proton resonance line.[19]

Within an error of ± 0.5 Gauss we have not observed an anisotropy of the linewidth of the proton resonance line. We suppose that be-

cause of the spatial distribution of the protons the second moment of the dipolar interaction of the proton spins is nearly independent of the field orientation.

Temperature dependence of the Overhauser shift

In Figure 6 two temperature ranges can be distinguished: For $T < 190$ K the Overhauser shift increases and for $T > 190$ K it decreases with increasing temperature. According to (1) and (3) ΔB_{ov} is proportional to $\mathcal{P}_o \cdot \overline{A}_{zz} \cdot S \cdot V$. Each of these four factors shows its specific temperature dependence:

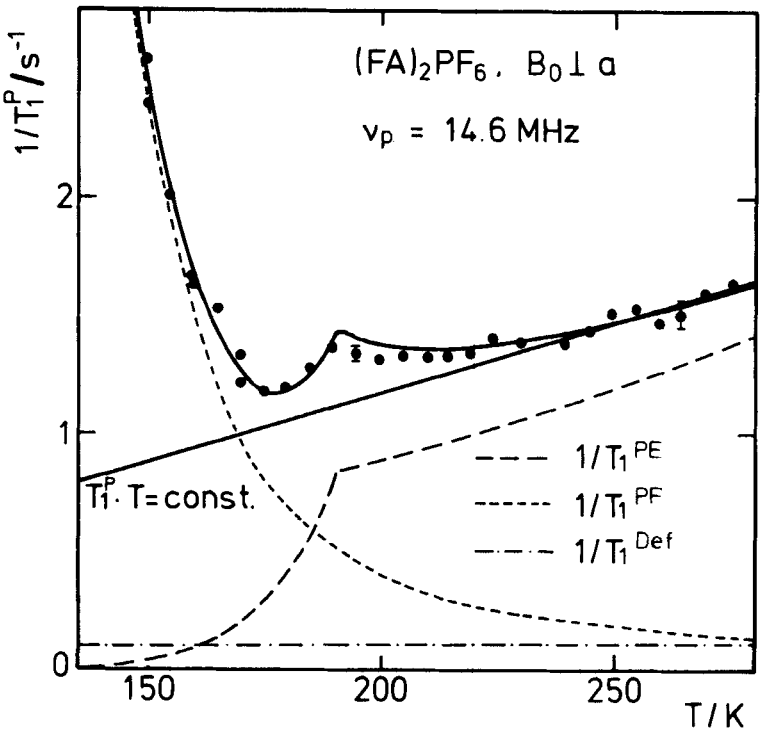

FIGURE 10 Temperature dependence of the longitudinal proton spin relaxation rate $1/T_1^p$. Dots: experimental values. Drawn out line: calculated as sum of the three parts:[33] proton–conduction electron rate $1/T_1^{PE}$, proton–fluor rate $1/T_1^{PF}$, and defect induced rate $1/T_1^{Def}$, respectively. The straight line represents a pure Korringa law $T_1^p \cdot T$ = const. This originally was published by Höptner et al.[16,31]

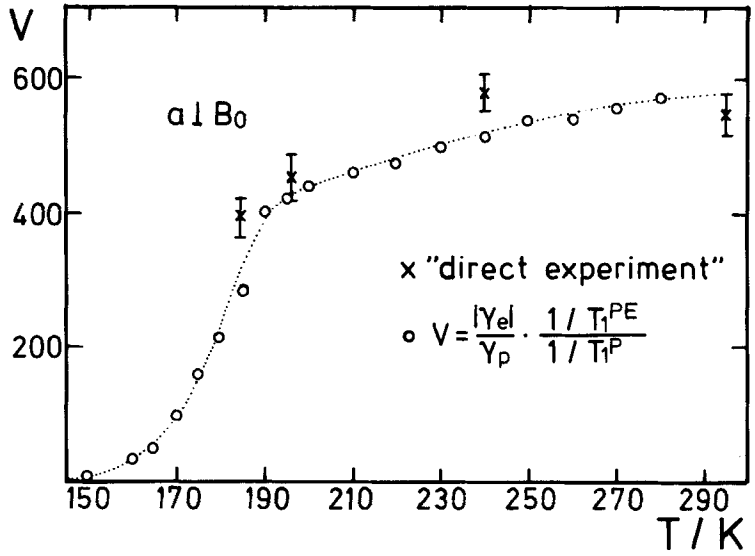

FIGURE 11 Temperature dependence of the enhancement factor V for $a \perp B_o$. x: experimental values from Figure 5, as detected from the microwave saturation of ΔB_{ov}. o: values calculated by Eq. (20) from the ratio of the relaxation rates $1/T_1^{PE}$ and $1/T_1^{p}$, respectively.

According to (6) we can put the enhancement factor into the following form:

$$V = \frac{w_2 - w_0}{w'} \cdot \frac{\gamma_e}{\gamma_p} \tag{19}$$

As shown above $w_2 \approx 0$ for $a \perp B_o$. Therefore in a first approximation

$$V = \frac{w_0}{w'} \cdot \frac{|\gamma_e|}{\gamma_p} \tag{20}$$

for $a \perp B_o$. The ratio w_o/w' can be determined directly by Figure 10. By (20) this yields $V(T)$, which is shown in Figure 11. For comparison Figure 11 also contains values of V which have been determined directly as described earlier. Thus, for $T > 190$ K the enhancement factor is nearly constant. For $T < 190$ K it decreases rapidly with decreasing temperature.

Multiplying the experimental values of the Overhauser shift with the temperature T for $T > 190$ K eliminates the (Curie $-$) temper-

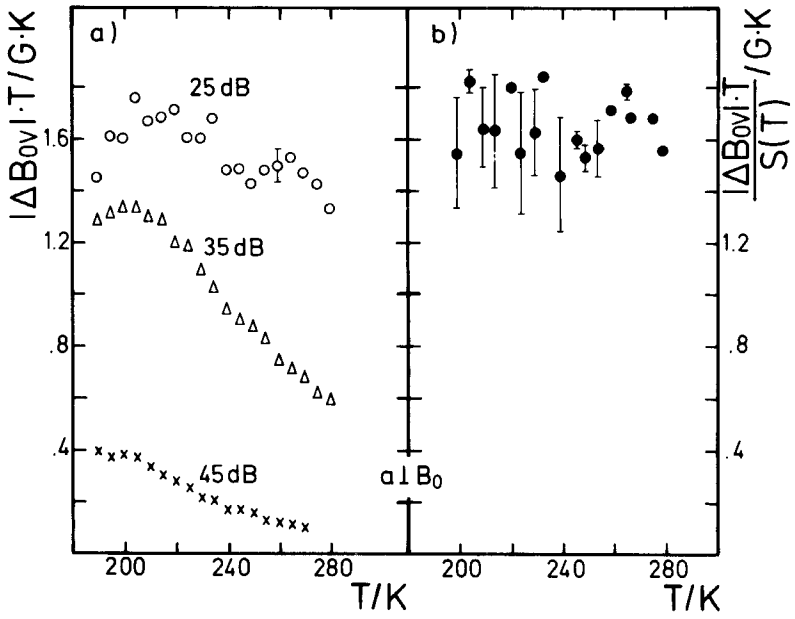

FIGURE 12 a) $\Delta B_{ov}(\nu_p) \cdot T$ versus T for different attenuations of the microwave power: 25 dB, 35 dB and 45 dB, respectively. (The multiplication of ΔB_{ov} with T compensates the temperature dependence of the thermal proton spin polarization $\mathcal{P}_o$). b) $\Delta B_{ov}(\nu_p) \cdot T/S(T)$ versus T. Each dot is the average of the corresponding values for all three microwave powers in a). (This representation compensates the temperature dependence of the saturation parameter S).

ature dependence of the thermal nuclear spin polarization $\mathcal{P}_o$: in Figure 12a this product $\Delta B_{ov} \cdot T$ is shown versus T for different values of the microwave power P. The remaining temperature dependence must be due to $S \cdot \overline{A}_{zz}$. As the electron spin relaxation times T_1^e and T_2^e are temperature dependent,[7,11,14] S is temperature dependent also. Figure 12b shows $\Delta B_{ov} \cdot T/S(T)$. Within the indicated error bars this product is constant. The temperature dependence of ΔB_{ov} therefore primarily is due to the temperature dependencies of S and $\mathcal{P}_o \cdot \overline{A}_{zz}$ however is constant for $T > 190$ K.

Below 190 K the strong decrease of V with decreasing temperature dominates the temperature dependence of the Overhauser shift.

VI. ABSOLUTE VALUE OF g_e

In this short chapter we will show that the g-value of the charge carriers can be detected via the Overhauser shift with high accuracy.

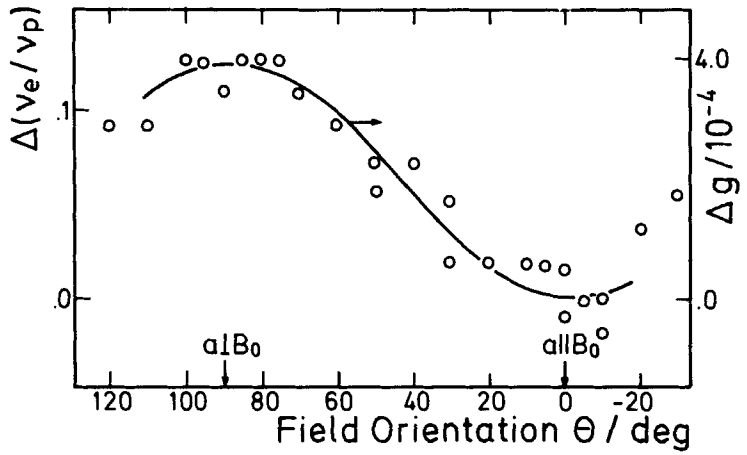

FIGURE 13 Anisotropy of the electron spin Larmor frequency. Dots: $\Delta(\nu_e/\nu_p) = (\nu_e(\theta) - \nu_e(0))/\nu_p$. Drawn out line: $\Delta g = g(\theta) - g(0)$.

This is due to two reasons: i) the ESR line is extremely narrow and ii) any conceivable shift due to demagnetization is eliminated in the Overhauser shift experiment: Figure 3 shows an NMR spectrum detected by ESR. Both Larmor frequencies, ν_p and ν_e are measured simultaneously and they are due to electron spins and proton spins inside the small crystal. I.e., even if a demagnetization field shift is

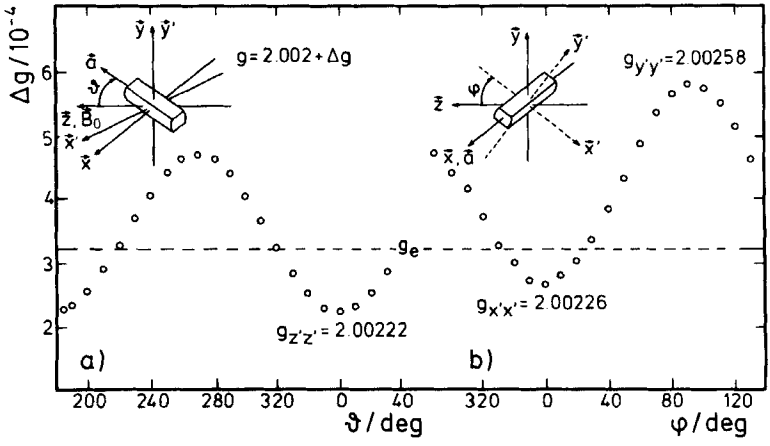

FIGURE 14 Anisotropy of the g-value of $(FA)_2PF_6$. For a) the crystal was rotated by the angle around an axis perpendicular to both, B_o and a. For b) the crystal was rotated by the angle around an axis perpendicular to B_o and parallel to a. The absolute values of g have been determined via the ratio ν_e/ν_p.

effective, it is eliminated for the ratio ν_e/ν_p. Thus g_e is determined using ν_p as an internal field probe via the relation

$$g_e = g_p \cdot \frac{\mu_N}{\mu_B} \cdot \frac{\nu_e}{\nu_p} = 2.0023 \cdot \frac{\mu_p}{\mu_e} \cdot \frac{\nu_e}{\nu_p} \tag{19}$$

Figure 13 shows the anisotropy of ν_e/ν_p. Assuming ν_p = const. this is the anisotropy of g_e. The direct detection of the anisotropy of g_e via cw ESR and external field measurement yields the same result (drawn out line in Figure 13).

The entire anisotropy of g_e is shown in Figure 14. The relative accuracy is $<10^{-5}$. The absolute values are $g_{xx} = 2.00226$, $g_{yy} = 2.00258$ and $g_{zz} = 2.00222$. Their absolute accuracy is $\pm 5 \cdot 10^{-5}$, resulting from the uncertainty of ν_p and μ_p.

VII. CONCLUSIONS

It has been shown so far that the Overhauser shift experiments are suitable to detect the hyperfine coupling constant $\overline{A}_{zz}$ and the proton spin relaxation times T_1^p and T_2^p, respectively for $(FA)_2PF_6$ crystals, the ESR line of which shows neither hyperfine splitting nor inhomogeneous broadening. As small single crystals produced strong enough signal to noise ratios we were able to measure anisotropies and temperature dependencies. Thus, fundamental interactions of the charge carriers in these organic conductors have been made accessible experimentally. The Overhauser shift method—similar to ENDOR—profits from the quantum transformation, resulting in a sensitivity which exceeds that of conventional NMR.

The method is not limited to $(FA)_2PF_6$ crystals. It requires only highly mobile electron spins and hyperfine coupled nuclei. It should therefore be possible to apply the method to other organic conductors, crystalline as well as polymeric ones. Narrow ESR lines, however, are favourable.

Also, the method is not limited to protons. For the $(FA)_2PF_6$ crystals we also tried to detect P and F. So far we only can set an upper bound: the ratio $\Delta B_{ov}(P \text{ or } F)/\Delta B_{ov}(H) < 5 \cdot 10^{-3}$. Even when taking into account the respective concentrations and the different Boltzmann factors this already confirms that the electrons mainly are restricted to the $(FA)_2$ stacks.

After having completed the experiments described above we have improved the sensitivity of the method. We are now able to detect

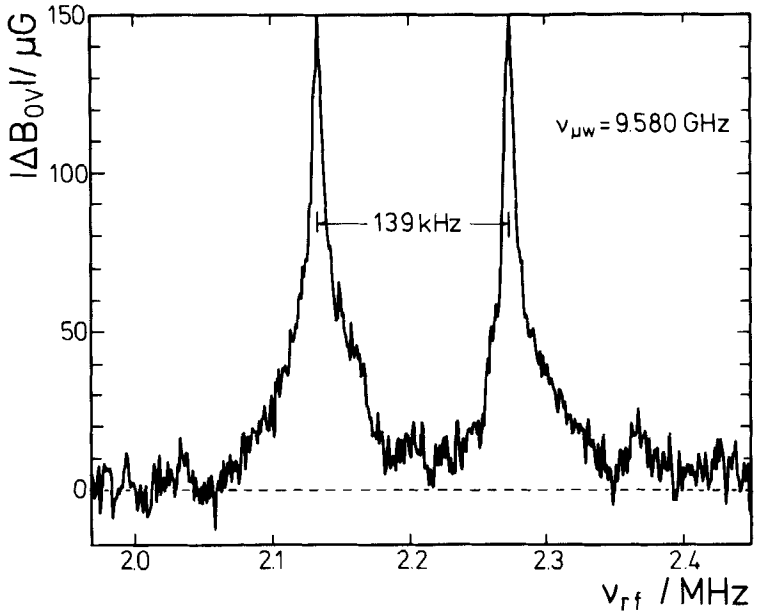

FIGURE 15 Quadrupole splitting as detected by the Overhauser shift $\Delta B_{ov}(\nu_{rf})$ for a perdeuterated $(FA)_2PF_6$ single crystal with B_o parallel to a.

relative shifts in the ppb range: $\Delta B_{ov}/B_o > 10^{-9}$! For example we have been able to detect ^{13}C in its natural abundance or ^{2}H in deuterated crystals. Figure 15 shows as an example the Overhauser shift spectrum for ^{2}H in a perdeuterated $(FA)_2PF_6$ single crystal. The splitting is the quadrupole splitting. The assignment to individual deuteriums will yield detailed information on the spin density.[19] The ^{13}C and ^{2}H data are complementary to the ^{13}C knight shift results obtained by Mehring and Spengler[32] which also give information on the intramolecular spin distribution.

Finally, we would like to point out that extreme care has to be taken in analyzing the lineshape of ESR signals the width of which is comparable to the expected Overhauser shift. Owing to the dynamic nature of the nuclear spin polarization, the ESR becomes asymmetric, especially at high Larmor frequencies, since the shift is expected to be proportional to the ESR frequency through the Boltzmann factor of the protons. This asymmetry is most pronounced near saturation, but even for power levels far from saturation the shift (and the resulting asymmetry) is not negligible. Under those conditions, a symmetric lineshape can only be observed either by saturating the protons

or by sweeping through resonance rapidly compared to the T_1^{ρ} time of the protons. Details will be published elsewhere.[19]

Acknowledgment

We thank Brigitte Kraus and J. Gmeiner for growing the single crystals, K. P. Dinse, J. U. v. Schütz and M. Mehring for helpful discussions. We are indebted to M. Schwoerer and E. Dormann for continuous support, many suggestions and stimulating discussions. This work has been supported by Stiftung Volkswagenwerk and in part also by the Deutsche Forschungsgemeinschaft (Sonderforschungsbereich 213, Bayreuth).

References

1. G. Wegner, *Angew. Chem.*, **93**, 352 (1981).
2. H. J. Keller, D. Nöthe, H. Pritzkow, D. Wehe, M. Werne, P. Koch and D. Schweitzer, *Mol. Cryst. Liquid Cryst.*, **6**, 181 (1980).
3. T. C. Chiang, A. H. Reddoch and D. F. Williams, *J. Chem. Phys.*, **54**, 2051 (1971).
4. H. P. Fritz, H. Gebauer, P. Friedrich, P. Ecker, R. Artes and U. Schubert, *Z. Naturforschung*, **B33**, 498 (1978).
5. W. Stöcklein, B. Bail, M. Schwoerer, D. Singel and J. Schmidt, *Organic Molecular Aggregates*, Proceedings of the International Symposium on Organic Materials at Schloβ Elmau, 228 (1983).
6. H. Eichele, M. Schwoerer, Ch. Kröhnke and G. Wegner, *Chem. Phys. Lett.*, **77**, 311 (1981).
7. G. Sachs, W. Stöcklein, B. Bail, E. Dormann and M. Schwoerer, *Chem. Phys. Lett.*, **89**, 179 (1982).
8. E. Dormann, *Physik. Blätter*, **39**, 220 (1983).
9. V. Enkelmann, B. S. Morra, Ch. Kröhnke and G. Wegner, *Chem. Phys.*, **66**, 303 (1982).
10. V. Enkelmann, *Habilitationsschrift*, Freiburg, (1983).
11. G. G. Maresch, M. Mehring, J. U. v. Schütz and H. C. Wolf, *Chem. Phys.*, **85**, 333 (1985).
12. J. Sigg, H. Prisner, K. P. Dinse, H. Brunner, D. Schweitzer and K. H. Hausser, *Phys. Rev.*, **B27**, 5366 (1983).
13. G. G. Maresch, A. Grupp, M. Mehring, J. U. v. Schütz and H. C. Wolf, *Journal de Physique*, **46**, 461 (1985).
14. W. Stöcklein, *thesis*, Bayreuth (1985).
15. D. Schiller, *Diplomarbeit*, Bayreuth (1984).
16. W. Höptner, M. Mehring, J. U. v. Schütz, H. C. Wolf, B. S. Morra, V. Enkelmann and G. Wegner, *Chem. Phys.*, **73**, 253 (1982).
17. G. Sachs, E. Dormann, M. Schwoerer, *Solid State Com.*, **53**, 73 (1985).
18. G. Denninger, W. Stöcklein, E. Dormann, M. Schwoerer, *Chem. Phys. Lett.*, **107**, 222 (1984).
19. G. Denninger, to be published (1985).
20. E. Dormann, G. Sachs, W. Stöcklein, B. Bail and M. Schwoerer, *Appl. Phys.* **A30**, 227 (1983).
21. G. Sachs and E. Dormann, *Bruker Report* (1984).
22. E. Dormann and U. Köbler, *Solid State Com.*, **54**, 1003 (1985).
23. E. Haindl, private communication.

24. A. W. Overhauser, *Phys. Rev.*, **89**, 689 (1953).
25. Ch. Ryter, *Phys. Rev.*, **5**, 10 (1960).
26. A. Abragam, "*Principles of Nuclear Magnetism*," Oxford, 375 (1973).
27. W. G. Clark, J. Hamman, J. Sanny and L. C. Tippie, "*Quasi One-Dimensional Conductors II*" Proceedings, Dubrovnik, 1978.
28. I. Solomon, *Phys. Rev.*, **99**, 559 (1955).
29. H. M. Mc. Connell and D. B. Chestnut, *J. Chem.*, **28**, 107 (1958).
30. A. Abragam, "*Principles of Nuclear Magnetism*," Oxford, 103 (1973).
31. W. Höptner, M. Mehring, J. U. v. Schütz, H. C. Wolf, B. S. Morra, V. Enkelmann, G. Wegner, *Mol. Cryst. Liq. Cryst.*, **93**, 395 (1983).
32. M. Mehring and J. Spengler, *Phys. Rev. Lett.*, **53**, 2441 (1984).
33. E. Dormann, private communication.